THESIS

NUCLEATION AND GROWTH: MODELING THE NH_3 - HCL REACTION

Submitted by

Jaime M. Shinn

Department of Mathematics

.

In partial fulfillment of the requirements

For the Degree of Master of Science

Colorado State University

Fort Collins, Colorado

Spring 2012

Master's Committee:

   Advisor: Patrick Shipman

   James Liu
   Jennifer Mueller
   Stephen Thompson

ABSTRACT

NUCLEATION AND GROWTH: MODELING THE NH_3 - HCL REACTION

One of the trademarks of a Liesegang ring system is the exhibition of a moving reaction front to form a periodic precipitation pattern. This phenomenon has been studied by both chemists and mathematicians. The periodic patterns produced have developed an interest from a mathematical perspective, while the theory and mechanism behind these patterns has created interest from a chemist's point of view. Many mathematical models have been proposed, and much interest has been invested in studying the mechanism behind these Liesegang ring systems. In particular, we will consider the NH_3-HCl system, a gas-phase system in which the two gases (NH_3 and HCl) diffuse into a tube and meet to form a solid precipitate. The reaction front then moves down the tube, forming a Liesegang banding pattern along the way. In this thesis, we derive a model for this system and examine some results of the model, which contribute to the theory and mechanism behind the NH_3-HCl system. We predict the position of the first and last Liesegang band formed, and we examine the effect of the tube length of our system. Front velocity data from the model has also been obtained and is shown to correlate well with experimental data. We also note that the width of the heterogeneous nucleation zone increases as the concentration ratio of NH_3 to HCl decreases, and we discuss the effect that water vapor has on the system.

ACKNOWLEDGEMENTS

TABLE OF CONTENTS

1 Introduction

Quentin leaned forward and shook his finger at me. "Listen, old man, if you don't work these equations, what will be the point of all we've done? We might end up building a good rocket that'll fly just fine, and all the grown-ups and teachers will brag on us. Who knows? We might even be able to bluff our way past the judges at the science fair. But you'll know and I'll know-all the boys will know-what could have been done if you hadn't lost your nerve. We could have built a great rocket."

"What's your definition of a great rocket?" I asked.

He crossed his arms and jutted out his chin. "One that does precisely what it's designed to do. It doesn't matter if it only flies two hundred feet. If that's what it's designed to do, and that's what it does, it will be a great rocket." He pointed at the book. "We want our rocket to go to an altitude of precisely two miles. The equations to make that happen are in that book. Do them!"

-excerpt from *Rocket Boys* by Homer H. Hickam, Jr. [12]

Periodic precipitation, or more specifically Liesegang rings, have been studied for many reasons. The patterns formed are a unique demonstration of precipitation in the presence of a moving reaction front. This unique pattern formation is important to the development of electro-optics, photonics, microreactors, and biosensors [17], and the formation of these patterns has been observed in polymer films and agate rocks [6]. It has also been found that this process is also important in the production of aerosols [2].

Traditionally, Liesegang ring experiments have been done in gels. Two chemicals react in the gel, and a moving reaction front is observed in the form of bands or rings. More details of this will be discussed in Section 2.1. It has been found that these Liesegang bands obey certain laws

(1) Time Law [19, 21]: $x_n = \sqrt{2D_f t_n}$

(2) Spacing Law [8, 14]: $\frac{x_{n+1}}{x_n} \to 1 + p$

(3) Width Law [8]: $w_n \sim x_n^\alpha$

where x_n is the n-th band position, D_f is the diffusion coefficient of the reaction front, w_n is the width of the n-th band, and p and α are constants. Certainly these Liesegang rings exhibit mathematically interesting behavior.

While most Liesegang systems occur in gels, we will focus on the NH_3-HCl system. Unlike traditional Liesegang ring experiments, the NH_3-HCl system is a gas-to-particle system. Diffusion through a medium still occurs, but rather than using a gel as our medium, we simply have ammonia (NH_3) and hydrochloric acid (HCl) diffusing through air as gases reacting to form solid particle. Details of this will be discussed in Section 2.4.

When we allow this diffusion to occur, we observe an interesting pattern of solid formation and then a period of little or no solid formation as we see in Figure 1. From this we can see that we have a moving reaction front. In fact, a moving reaction front has been observed even if visible rings do not form [18].

Figure 1: The results of an NH_3-HCl experiment. The two gases diffuse into the tube from either side until they meet and react. The reaction front moves down the tube, and Liesegang banding pattern is observed.

In this thesis, we will begin with an introduction of Liesegang rings, nucleation theory, and the NH_3-HCl system, the Liesegang ring system that will be our focus. We will then give a complete derivation of our model for the NH_3-HCl system. Some results of our model will be stated and discussed, including results discussing band position, front position, front velocity, the effect of changing the tube length, and the effect that water vapor has on the system. Finally, we will end with a discussion of ideas for future work.

2

2   Pattern Formation

2.1   Liesegang rings

We begin with the topic of Liesegang rings, named after the man who studied this periodic precipitation pattern, R.E. Liesegang. Liesegang discovered these rings when he placed a drop of ammonium dichromate ($(NH_4)_2Cr_2O_7$) onto a gel containing silver nitrate ($AgNO_3$) [19]. The two chemicals reacted to form silver dichromate and in doing so, formed a rather interesting pattern, as shown in Figure 2. Here we see periodic precipitation and true Liesegang rings.
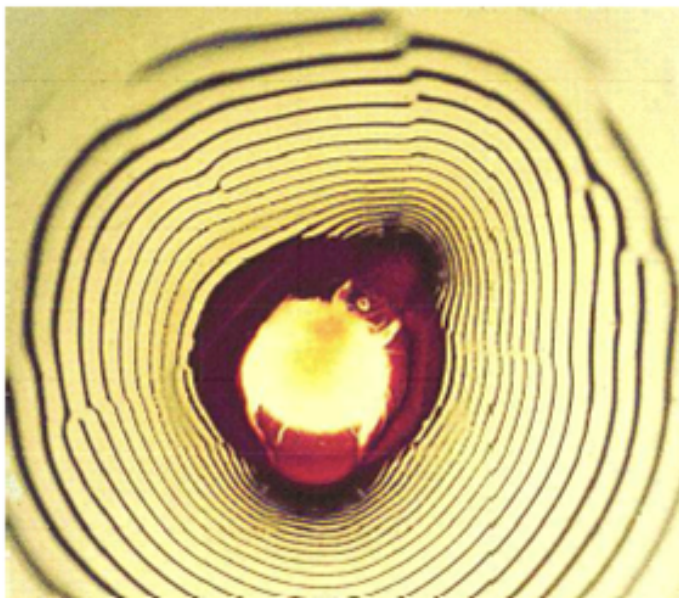
Figure 2: Liesegang rings formed on a gel containing $AgNO_3$. The $(NH_4)_2Cr_2O_7$ drop can be seen in the middle, and a moving reaction front is observed through periodic precipitation [19].

If we change the geometry of the experiment, we can get different geometric patterns. Depending on the set-up of the experiment, we can get rings, bands, and even spherical shells [19]. The commonality between all of these systems is that they are all reaction-diffusion systems. The

chemicals react and form a band, ring, or shell of the product. Then we observe a period where the the reaction front moves (because of diffusion), and then the chemicals react again to form another ring or band. The process then simply repeats over and over again. Interestingly enough, this general reaction-diffusion process is the same mechanism that causes zebras and fish to be striped and leopards to be spotted [19].

Traditionally, these Liesegang experiments are done in a gel and often in test tubes. When these experiments are done in test tubes, Liesegang bands are obtained, as we can see in Figure 3. We will focus on the tube geometric configuration since the experiment discussed in this thesis is performed in a horizontal tube.

Figure 3: Liesegang bands in test tubes [27].

In the tube experiments, generally a tube is filled with a gel which contains one of the reactants. Then, the other chemical, as an aqueous solution is placed on the top of the gel (in the case of a vertical test tube) or on one or both ends of the tube (in the case of a horizontal test tube). The chemicals react, and the reaction front travels down the tube, forming bands along the way. The question of how and why these patterns form will be addressed in the next section.

2.2　Nucleation and Growth

Several theories have been presented on why and how Liesegang rings form. The mechanisms involved include diffusion, reaction, nucleation, and growth, as a phase transformation occurs. There are many different theories as to what exactly occurs at the molecular level during these reactions. Therefore, before we discuss the mathematical equations used to model this system, let us first discuss some of the chemistry behind Liesegang rings.

We first begin with a discussion of the Gibbs free energy of the system. In Liesegang ring systems, generally, a precipitate is formed from two diffusing chemicals. In our system that we will consider, this is indeed the case, and we will see in Section 2.4 that we actually have two gases diffusing together to form a solid precipitate. In order for this reaction to occur, supersaturation must take place. In the process of going from a gas to a solid, molecules in the gaseous form must essentially bind together to form a cluster, or solid particle. In doing so, we must consider both the molecules that are now on the surface of this cluster and the molecules that are positioned in the inner bulk of this cluster.

We may think of the change in Gibbs free energy, or ΔG, as a measurement of the stability of a system. If we think of the bulk and surface molecules of our solid precipitate in these terms, we obtain a graph of the ΔG of our system as shown in Figure 4. Notice that the molecules which go from gas to solid as bulk molecules become more stable, as we see with the decreasing bulk term line, while the the surface molecules actually become less stable, exhibited by the surface term curve. This occurs because creating surface requires energy. The molecules on the surface of a particle will not be as stable as molecules in the bulk of the particle.

Now consider the overall stability of the entire cluster including both the surface and bulk molecules. In Figure 4, this is represented by the solid curve, ΔG_n^o, where the ^{o} denotes the standard Gibbs free energy. Notice that our cluster will at first become less stable until it reaches a certain point $(n^*, \Delta G^*)$, the nucleation point, where the cluster has overcome the energy barrier, and after this point, the cluster will then become more and more stable. The initial instability is caused by the surface molecules and the energy required to create surface. Eventually, though, stability of the bulk molecules will cause the cluster to be in a much more stable state that it was in originally.
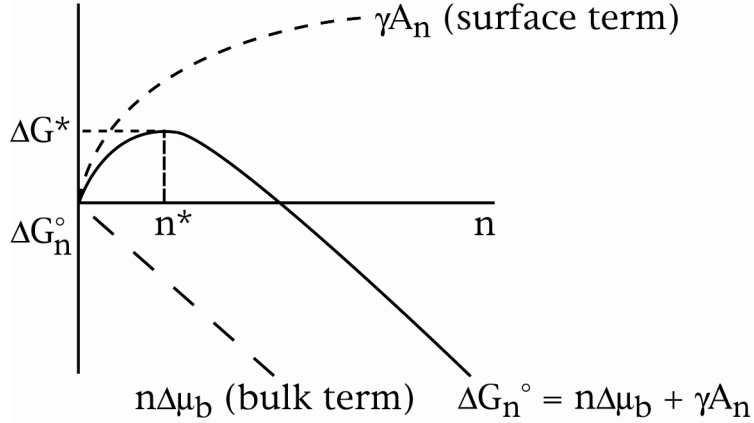
Figure 4: Change in Gibbs free energy (ΔG) vs. Number of molecules (n). We call ΔG^* the energy barrier to nucleation and n^* the number of particles in a critical cluster [18].

The question still remains, though, about how the bands in the NH$_3$-HCl system (as shown in Figure 2) are actually formed. For this discussion, we will refer to Figure 5. We understand from Figure 4 that the nucleation point, $(n^*, \Delta G^*)$, is an an essential part of this process since we must reach this point before we obtain a stable cluster. Then let us consider the rate of nucleation, J, of our critical clusters. Notice that as the concentration of our molecule (C) increases, the rate of nucleation increases as well but very slowly at first. This is where heterogeneous nucleation (nucleation initiated by things such as dust particles and walls) occurs. Then, once the molecule concentration has increased just enough to reach the point S_{crit}, we see a sharp, almost instantaneous, increase in the nucleation rate. It is here where we observe the onset of homogeneous nucleation, where the molecule nucleates with other molecules or on previously formed solid particles, as described in the discussion of Figure 4.

This sharp increase in nucleation rate is important, but it alone does not explain the banding pattern that we observe. Recall that the two chemicals will diffuse into the tube. Then, once they meet, as long as this happens quickly, we will see a sudden burst of precipitate once we have reached the critical threshold S_{crit}. Then the reaction front will move, due to differences in the diffusion coefficients and differences in the concentrations of our reactants, and the process will begin all over again. It continues in this pattern: a burst of solid precipitate, followed by a movement of the reaction front, as shown in Figure 6 .

Now that we understand the general mechanism behind Liesegang rings and specifically our
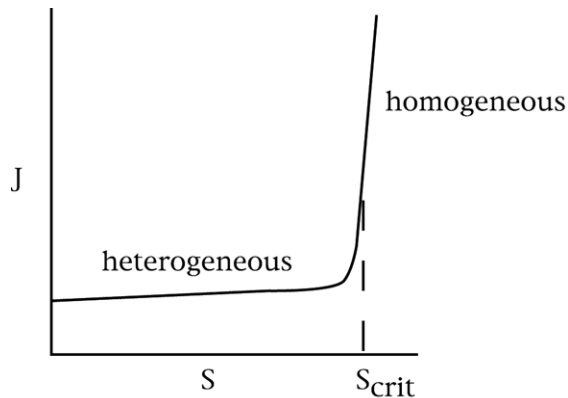
Figure 5: Rate of nucleation (J) vs. Supersaturation ratio ($S = \frac{C}{C_0}$), where C_0 is the supersaturation concentration [18].
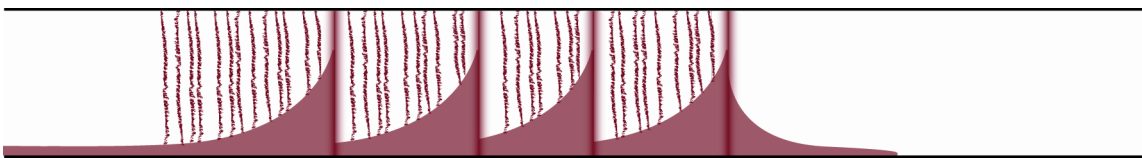
Figure 6: The build-up, the burst of precipitate, and the Liesegang bands which are left behind as the reaction front moves to the right. This process will occur over and over as we travel up and down the curve in Figure 5 [18].

NH$_3$-HCl system, we can focus on the nucleation threshold, S_{crit}. If we let $a =$ the concentration of one of the diffusing chemicals, and $b =$ the concentration of the other, many models measure S, the supersaturation ratio, with respect to the quantity $a * b$ [1, 11, 17] . As we will see, we will measure S with respect to the concentration of the monomer formed when our two chemcials react. Details of this will be discussed later when we describe the model itself.

2.3   Existing Pre-nucleation Models

Many models of Liesegang rings are present in the literature. Here, we choose to focus on the pre-nucleation models of Dee, Lebedeva *et al.*, Antal *et al.* and Hantz, and Einarsrud. We begin with the model developed by Dee.

$$a_t = a_{xx} - \kappa ab$$

$$b_t = \frac{D_b}{D_a}b_{xx} - \kappa ab$$

7

$$s_t = \frac{D_s}{D_a} s_{xx} + \kappa ab - u$$

Here, a and b represent the concentrations of the two reactants, s the concentration of the product formed, and D_a, D_b, and D_s the respective diffusion coefficients. κ is the scaled reaction rate constant, and u describes the depletion of the product s [6].

Next we consider the model developed by Lebedeva *et al.*

$$a_t = a_{xx} - \kappa ab(H(ab - I_0) + \gamma s^\nu)$$

$$b_t = \frac{D_b}{D_a} b_{xx} - \sigma \kappa ab(H(ab - I_0) + \gamma s^\nu)$$

$$s_t = \sigma \kappa ab(H(ab - I_0) + \gamma s^\nu)$$

We see some similarities with the Dee model, but notice that Lebedeva *et al.* have incorporated a threshold value I_0 and have modeled that threshold behavior using a Heaviside step function $H(ab - I_0)$. Note that this threshold is determined by the amount ab. They have also modeled the effect of autocatalytic growth of the product s by the γs^ν term [17].

We may also consider the model presented by Antal *et al.* and Hantz.

$$a_t = D_a a_{xx} - \gamma H(ab - I_0) - \lambda abs$$

$$b_t = D_b b_{xx} - \gamma H(ab - I_0) - \lambda abs$$

$$s_t = \gamma H(ab - I_0) + \lambda abs$$

Notice again that the threshold behavior is determined by the quantity ab. We also see that an aggregation term, λabs, has been incorporated [1, 11].

The three models described above have been for Liesegang ring systems in a general sense. Now we turn our attention to a model by Einarsrud *et al.* which focuses on the NH_3-HCl system specifically.

$$a_t = D_a a_{xx} - Rab$$

$$b_t = D_b b_{xx} - Rab$$

$$c_t = D_c c_{xx} + Rab - N_1 H(c - c_0)c^2 - N_2 cs$$

$$s_t = N_1 H(c - c_0)c^2 + N_2 cs$$

Notice that we now have four equations since this model takes into account an intermediate product c. Note, now, that the threshold behavior is determined by this intermediate product c, rather than ab, as in the previous two models [9]. It is important to note that this experiment was carried out in a gel, unlike the NH_3-HCl system that we will study, as we will see in Section 2.4.

2.4 The NH_3 - HCl System

A popular high school chemistry experiment consists of placing aqueous hydrochloric acid (HCl) at one end of a long tube and aqueous ammonia (NH_3) at the other end and letting the two gases diffuse into the tube. The gases then meet and react to form NH_4Cl, a solid precipitate. This first reaction produces the first band of solid precipitate. As we observed in Figure 1, many other bands may form after the initial band, but for this high school experiment, the focus is on the position of the first band. Students then measure the distance from the ends of the tube to this band, and they claim to observe that the ratio of the distances is equal to the square root of the ratio of the molecular weights of HCl and NH_3 [20];

$$\frac{L_{NH_3}}{L_{HCl}} = \sqrt{\frac{M_{HCl}}{M_{NH_3}}} = 1.47. \tag{1}$$

The intention of this experiment is to demonstrate Graham's Law of Diffusion. However, as Lenczycki and Mason and Kronstadt have pointed out, this is an incorrect interpretation of Graham's Law of Diffusion [18, 20]. If we can show that the position of the first ring changes by varying certain conditions (such as changing the concentration of NH_3 and HCl at the ends of the tube), then we will be able to further support the claims of Lenczycki, Mason and Krondstadt.

Now let us discuss the details of our NH_3-HCl experiment in the context of our model. We will discuss only the details that are necessary for the model. For more details of the set-up of this experiment, I will refer the reader to Timothy Lenczycki's thesis [18].

We begin with a tube of length L (in cm) with hydrochloric acid (HCl) solution capped on one end of the tube at $x = 0$ and ammonia (NH_3) solution on the other end at $x = L$. Let us

assume that the concentration of HCl, a_0, and the concentration of NH$_3$, b_0, at the ends both stay constant. We will consider two different experiments. The first we will call the **counter-diffusional experiment**. In this experiment, at $t = 0$, we cap the ends of the tube with these chemicals and let the two gases diffuse into the tube until they meet and start to react. This experiment is illustrated by Figure 7. We will call the second experiment the **flooded tube experiment**. This experiment has the exact same set-up except that at $t = 0$, we not only have the HCl and NH$_3$ at the ends of the tube, but we also flood the tube completely with HCl gas at the same concentration, a_0.
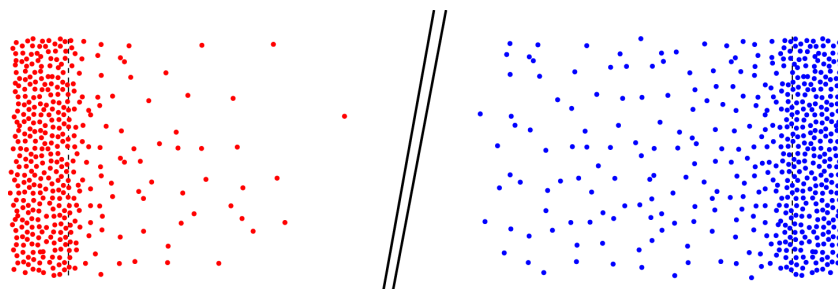
Figure 7: The counter-diffusional experiment. The HCl at $x = 0$ diffuses into the tube from the left, and the NH$_3$ at $x = L$ diffuses in from the right [18].

Once the two chemicals meet and react, we will see a moving reaction front. If we model this correctly, we should be able to observe band formation at the reaction front, followed by a period of less precipitate while the reaction front is moving, followed by another band of precipitate, and so on, as exhibited in Figure 6. In fact, this has been observed [18]. From hetereogeneous nucleation to homogeneous nucleation to a moving reaction front, these observations are detailed below in Figures 8 - 16. Figures 8 - 13 can only be seen when we shine a laser across the tube. All graphics are taken, with permission, from Timothy Lenczycki's Master's thesis [18].
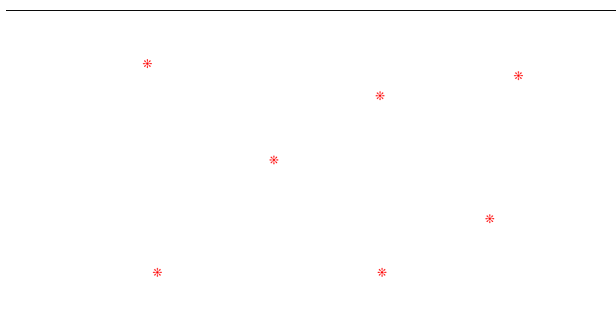
Figure 8: The first sign of hetereogeneous nucleation. Crystal particles begin to form.
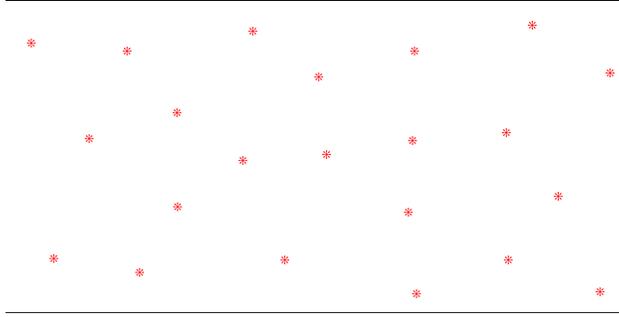
Figure 9: A heterogeneous nucleation zone forms. The width of this zone can be measured.
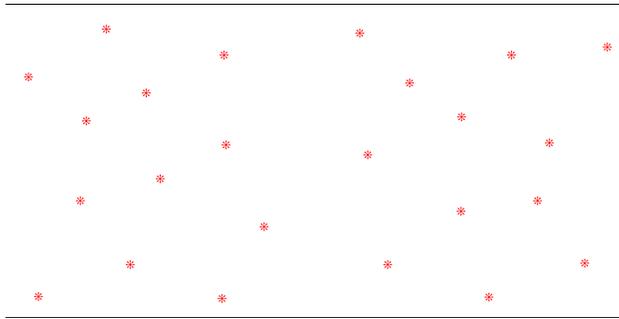
Figure 10: A depletion zone begins to form in the center of the heterogeneous nucleation zone.
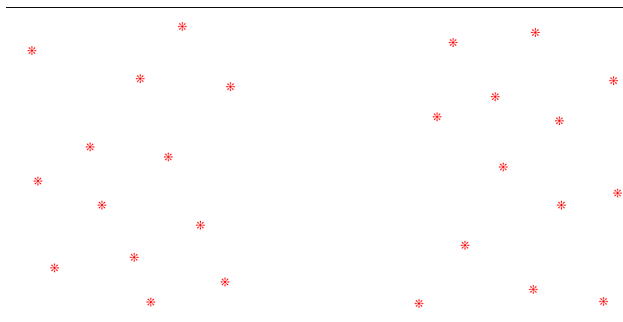
Figure 11: The depletion zone becomes more clear.
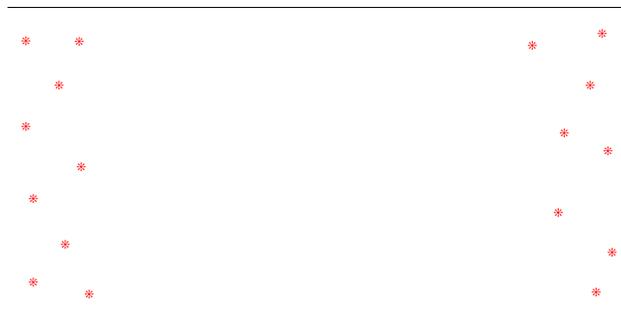
Figure 12: The depletion zone widens.
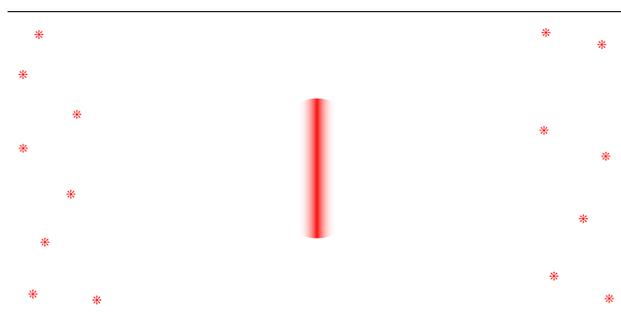
Figure 13: A small patch of light forms in the center of the depletion zone.

Figure 14: A reaction front begins to form.
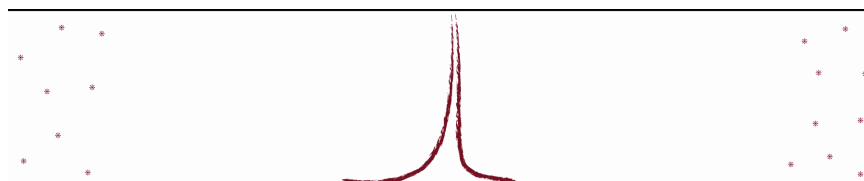
Figure 15: Solid precipitate builds up and is deposited.

Figure 16: The front moves down the tube, depositing solid precipitate along the way.

In our model, we will only consider a very basic mechanism for what is occurring. There are many theories about exactly what is occurring at the molecular level, but for our model, we will consider the following chemical equations:

$$NH_3 \ (g) + HCl \ (g) \xrightarrow{k_1} NH_4Cl \ (g) \quad \text{(Monomer Formation)} \tag{2}$$

$$NH_4Cl \ (g) + NH_4Cl \ (g) + \cdots + NH_4Cl \ (g) \xrightarrow{k_2} NH_4Cl \ (s) \quad \text{(Nucleation)} \tag{3}$$

$$NH_4Cl \ (g) + NH_4Cl \ (s) \xrightarrow{k_3} NH_4Cl \ (s) \quad \text{(Growth)} \tag{4}$$
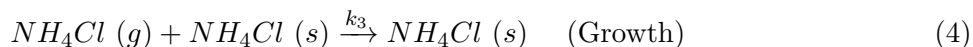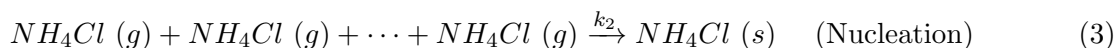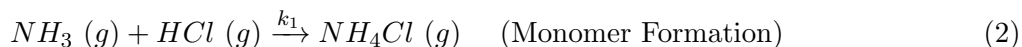
The first equation describes the formation of the monomer NH_4Cl (g). In our model, this is the quantity we will use to measure S as in Figure 5. The concentration of this monomer will help us to determine where the sharp increase in J, the rate of nucleation, will occur. For further discussion of this idea, see Section 3.3. The second equation describes that process shown in Figure 4, where after a certain, criticial number, n^*, of monomers have formed, the gaseous monomers join together to form a solid cluster or precipitate. This idea will also be discussed further when we develop our model. Finally, the third equation represents a monomer attaching itself to an already solidified cluster. This equation can be thought of in the context of post-nucleation, which we will discuss in Section 3.4.

Certainly, we have something here which exhibits pattern formation in the form of Liesegang bands. We would like to create a mathematical model which will give us some qualitative results and possibly some quantitative results as well. Then, rather than setting up an experiment each time that we want to change a parameter, we may be able to simply run a simulation of the experiment and from that, be able to make some predictions and decide what experiments would be best to run. Then we would have access to a whole spectrum of different parameters. In addition, we

will also be able to compare our model with the various modern theories about the formation of Liesegang rings.

We have several questions that we would like to answer with this model. Some of those questions include the following:

(1) Where does the first ring occur? (Section 4.1)

(2) Where does the last ring occur? (Section 4.2)

(3) What is the effect of changing the tube length L? (Section 4.3)

(4) What conditions cause the front to move towards the HCl or towards the NH_3? Can we find the conditions that cause the front to not move at all? (Figures 18 and 19)

(5) How does the width of the hetereogeneous nucleation zone depend on the concentrations of HCl and NH_3 at the ends of the tube? (Section 4.5)

(6) Since water is a catalyst in this reaction, what effect does it have on the system? (Section 4.6)

(7) Can we get our model to match experimental data? (Sections 4.1, 4.4, and 4.6)

3 The Model

3.1 Derivation of Diffusion Equation

Certainly, the set-up of this experiment, with a cylindrical rod and gases diffusing in from either end of the tube should encourage us to consider the diffusion equation. Let us therefore derive the diffusion equation in this context.

We first consider the flux of the gases; i.e., the amount of chemical that flows through any given cross-sectional area of our tube per unit time. In the case of our experiment, flux will be measured in units of $\frac{mol}{cm^2*s}$ Fick's law of diffusion then gives us

$$J = -D\frac{\partial \phi}{\partial x} \tag{5}$$

where J is the flux, D is the diffusion coefficient (a constant specific to the chemical/temperature), and ϕ is the chemical concentration. Notice that we obtain the desired units for flux since

$$[D] = \frac{cm^2}{s}, \quad [\phi] = \frac{mol}{cm^3}, \quad \text{and} \quad [x] = cm.$$

Now we take any points a and b along our tube, then by conservation of mass, we must have

$$\frac{d}{dt}\int_a^b \phi(x)\,dx = -J(b,t) + J(a,t).$$

By the Fundamental Theorem of Calculus, the right hand side of this equation becomes

$$-\int_a^b \frac{\partial J}{\partial x}\,dx,$$

and, as long as $\phi(x,t)$ is continuous (which it will be in our experiment), the left-hand side will become

$$\int_a^b \frac{\partial \phi}{\partial t} \, dx.$$

Therefore we have

$$\int_a^b \frac{\partial \phi}{\partial t} \, dx = -\int_a^b \frac{\partial J}{\partial x} \, dx \qquad \text{or} \qquad \int_a^b \left(\frac{\partial \phi}{\partial t} + \frac{\partial J}{\partial x} \right) dx = 0.$$

Since points a and b were chosen arbitrarily along the tube, then we must have that

$$\frac{\partial \phi}{\partial t} + \frac{\partial J}{\partial x} = 0 \quad \text{and therefore} \quad \frac{\partial \phi}{\partial t} = -\frac{\partial J}{\partial x}.$$

By (5), then we have

$$\frac{\partial \phi}{\partial t} = -\frac{\partial}{\partial x} \left(-D\frac{\partial \phi}{\partial x} \right)$$
$$= D\frac{\partial^2 \phi}{\partial x^2} \quad \text{since } D \text{ is a constant.}$$

Thus, in order to model the behavior of the gases in our model, HCl (g), NH_3 (g), and NH_4Cl (g), we will use the diffusion equation in one dimension:

$$\frac{\partial \phi}{\partial t} = D\frac{\partial^2 \phi}{\partial x^2}.$$

3.2   Chemical Kinetics

Now that we understand how the gases in our system will behave, we now must determine how to model the interactions and reactions of our chemicals. The simplest and first thing we will consider when modeling these reactions is the Law of Mass Action.

For an $mA + nB \to pC$ reaction with rate constant k, the Law of Mass Action states that the reaction rates will be

$$\frac{dA}{dt} = -mkA^m B^n$$
$$\frac{dB}{dt} = -nkA^m B^n$$
$$\frac{dC}{dt} = pkA^m B^n.$$

In other words, the rate of the reaction is only dependent upon k, m, n, p, and the concentrations of the reactants, A and B. If this reaction were reversible, $mA + nB \rightleftharpoons pC$, with k_1, the forward reaction rate constant and k_2, the reverse reaction rate constant, then our reaction rates would be

$$\frac{dA}{dt} = -mk_1 A^m B^n + mk_2 C$$
$$\frac{dB}{dt} = -nk_1 A^m B^n + nk_2 C$$
$$\frac{dC}{dt} = pk_1 A^m B^n - pk_2 C.$$

Notice that, just like above, the reverse reaction rate only depends on k_2 and the concentration of the reactant, C.

In our model, for simplification, we will only consider the forward reaction, although many sources have considered the reverse reaction as well [4, 15, 16]. If we combine our diffusion results with the law of mass action, assuming that our reaction has a 1:1:1 stoichiometric ratio, we obtain the following model:

$$\frac{\partial a}{\partial t} = D_a \frac{\partial^2 a}{\partial x^2} - k_1 ab \tag{6}$$

$$\frac{\partial b}{\partial t} = D_b \frac{\partial^2 b}{\partial x^2} - k_1 ab \tag{7}$$

$$\frac{\partial s}{\partial t} = k_1 ab, \tag{8}$$

where a represents HCl, b represents NH_3, and s represents the NH_4Cl solid that is formed from these two gases. But of course, our chemical equations are not that simple. The above equations would apply if we were only trying to model the simple chemical reaction NH_3 (g) + HCl (g) $\rightarrow$ NH_4Cl (s) with reaction rate constant k_1. From our chemical equations (2), (3), and (4), we see that this is not the case. We are dealing with a much more complicated system.

3.3 Incorporating the J-curve

Now that we have a basic model in equations (6), (7), and (8), let us now work on some of the details. At this point in our model, we have yet to incorporate all of the ideas from the chemical equations (2), (3), and (4) and also from Figures 4 and 5.

From equation (2), we must consider the intermediate step involving the monomer, m, in our model. Since the monomer is a gas, we can model it with the diffusion equation:

$$\frac{\partial a}{\partial t} = D_a \frac{\partial^2 a}{\partial x^2} - k_1 ab$$

$$\frac{\partial b}{\partial t} = D_b \frac{\partial^2 b}{\partial x^2} - k_1 ab$$

$$\frac{\partial m}{\partial t} = D_m \frac{\partial^2 m}{\partial x^2} + k_1 ab.$$

Then from equation (3), the nucleation equation where a solid particle is formed, by the Law of Mass Action we have

$$\frac{\partial a}{\partial t} = D_a \frac{\partial^2 a}{\partial x^2} - k_1 ab$$

$$\frac{\partial b}{\partial t} = D_b \frac{\partial^2 b}{\partial x^2} - k_1 ab$$

$$\frac{\partial m}{\partial t} = D_m \frac{\partial^2 m}{\partial x^2} + k_1 ab - k_2 m^\nu$$

$$\frac{\partial s}{\partial t} = k_2 m^\nu,$$

where ν is the number of monomers is takes to form the solid cluster. This ν is the same as the n^*, the number of molecules it takes to overcome the energy barrier ΔG^*, in Figure 4.

However, we still need to incorporate the J-curve from Figure 5 in to our model. If we recall that J is the *rate* of nulceation, then let us model the J-curve as part of the rate constant k_2. From Section 2.3, we see that Einarsrud mutiplied k_2 by the Heaviside function $H(m-\eta)$ to obtain a new rate constant $k_2 H(m-\eta)$ [9]. Here, when the monomer concentration is below some number η, the rate constant will be zero, but when the monomer concentration goes above η, the rate constant will be k_2. In other words, the Heaviside function acts like an on-off switch for the reaction to occur.

We will use something similar, except that instead of a discontinuous step function, we will use a continuous piecewise function as shown in Figure 17. This way, if we can find η, the point where we see the first signs of homogeneous nucleation to form a cluster, we can model the steep but

continuous increase of the J-curve. And so we obtain a model that incorporates the J-curve:

$$\frac{\partial a}{\partial t} = D_a \frac{\partial^2 a}{\partial x^2} - k_1 ab$$

$$\frac{\partial b}{\partial t} = D_b \frac{\partial^2 b}{\partial x^2} - k_1 ab$$

$$\frac{\partial m}{\partial t} = D_m \frac{\partial^2 m}{\partial x^2} + k_1 ab - k_2 H(m - \eta) m^\nu$$

$$\frac{\partial s}{\partial t} = k_2 H(m - \eta) m^\nu.$$
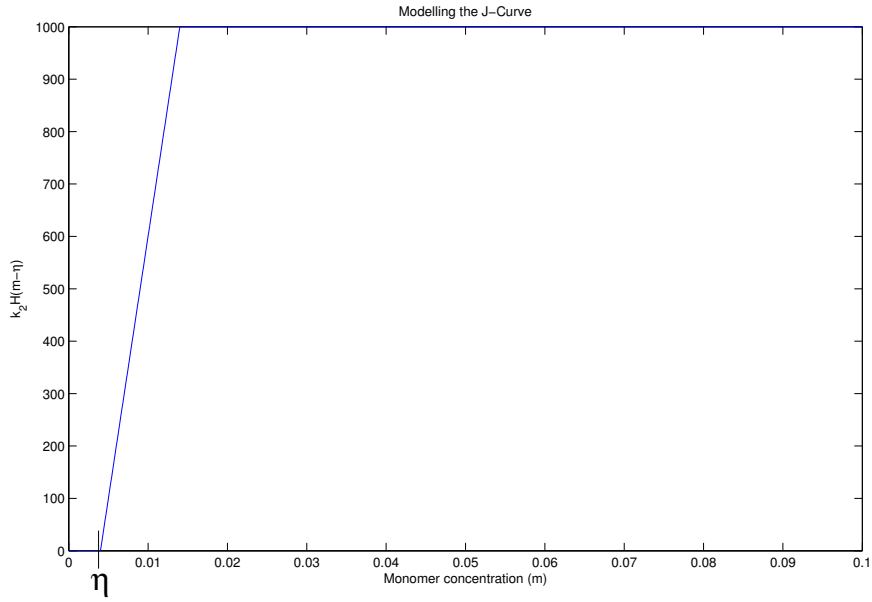
Figure 17: If $k_2 = 1000$, this is what our rate curve for $k_2 H(m - \eta)$ would look like.

Now notice here that we have chosen to measure S with respect to the quantity m instead of ab as Antal et $al.$, Hantz, and Lebedeva use [1, 11, 17] (See Section 2.3). If we were to measure S with respect to ab, our model would look like the following instead:

$$\frac{\partial a}{\partial t} = D_a \frac{\partial^2 a}{\partial x^2} - k_1 H(ab - \eta) ab$$

$$\frac{\partial b}{\partial t} = D_b \frac{\partial^2 b}{\partial x^2} - k_1 H(ab - \eta) ab$$

$$\frac{\partial m}{\partial t} = D_m \frac{\partial^2 m}{\partial x^2} + k_1 H(ab - \eta) ab - k_2 m^\nu$$

$$\frac{\partial s}{\partial t} = k_2 m^\nu.$$

19

3.4   Modeling Growth and the Final Set of Equations

Our model now accounts for the first two chemical equations, (2) and (3), so let us now take the third equation into account. This equation models the growth step where a monomer attaches itself to an already-formed solid cluster. Again, here we use the law of mass action to obtain:

$$\frac{\partial a}{\partial t} = D_a \frac{\partial^2 a}{\partial x^2} - k_1 ab$$

$$\frac{\partial b}{\partial t} = D_b \frac{\partial^2 b}{\partial x^2} - k_1 ab$$

$$\frac{\partial m}{\partial t} = D_m \frac{\partial^2 m}{\partial x^2} + k_1 ab - k_2 H(m - \eta)m^\nu - k_3 ms$$

$$\frac{\partial s}{\partial t} = k_2 H(m - \eta)m^\nu + k_3 ms.$$

Notice that, from Section 2.3, we see that Einarsrud uses this model with $\nu = 2$ [9].

Finally, we include the precipitate fallout by adding the term $-k_4 s$ to the last equation in our model. This accounts for the solid particles that stick to the walls, fall to the bottom of the tube, etc. Hence we obtain our final model for our system:

$$\frac{\partial a}{\partial t} = D_a \frac{\partial^2 a}{\partial x^2} - k_1 ab$$

$$\frac{\partial b}{\partial t} = D_b \frac{\partial^2 b}{\partial x^2} - k_1 ab$$

$$\frac{\partial m}{\partial t} = D_m \frac{\partial^2 m}{\partial x^2} + k_1 ab - k_2 H(m - \eta)m^\nu - k_3 ms$$

$$\frac{\partial s}{\partial t} = k_2 H(m - \eta)m^\nu + k_3 ms - k_4 s.$$

In our model, we will assume that $k_1 >> D_a, D_b$ [9, 30], and we will use the following parameter values:

* $D_a = 0.16 \frac{cm^2}{s}$ [7]

* $D_b = 0.23 \frac{cm^2}{s}$ [31]

* $D_m = 0.095 \frac{cm^2}{s}$ (calculated based on D_a and D_b)

3.5 Initial and Boundary Conditions

We would like to nondimensionalize our system of equations, but before we can do so, let us define our initial and boundary conditions. Recall that we are trying to model two different experiments: the flooded tube experiment and the counter-diffusional experiment. In both cases, we will have the same boundary conditions;

$$a(0,t) = a_0 \quad a_x(L,t) = 0$$

$$b(L,t) = b_0 \quad b_x(0,t) = 0$$

$$m_x(0,t) = 0 \quad m_x(L,t) = 0$$

$$s_x(0,t) = 0 \quad s_x(L,t) = 0.$$

However, we will have different initial conditions since for the flooded tube experiment, we initially flood the tube with HCl, whereas in the counter-diffusional experiment, we do not. Therefore, for the flooded tube experiment, we will have the following initial conditions:

$$a(x,0) = a_0 \quad b(x,0) = 0 \quad m(x,0) = 0 \quad s(x,0) = 0.$$

But for the counter-diffusional case, we will have

$$a(x,0) = 0 \quad b(x,0) = 0 \quad m(x,0) = 0 \quad s(x,0) = 0.$$

For the nondimensionalization of the system, we will only consider the flooded tube initial conditions, but notice that it would be quite easy to consider the counter-diffusional case as well.

3.6 Nondimensionalization

Now for our nondimensionalization, we will consider the following model:

$$\frac{\partial a}{\partial t} = D_a \frac{\partial^2 a}{\partial x^2} - k_1 ab$$

$$\frac{\partial b}{\partial t} = D_b \frac{\partial^2 b}{\partial x^2} - k_1 ab$$

$$\frac{\partial m}{\partial t} = D_m \frac{\partial^2 m}{\partial x^2} + k_1 ab - k_2 H(m - \eta)m^\nu - k_3 ms$$

$$\frac{\partial s}{\partial t} = k_2 H(m - \eta)m^\nu + k_3 ms - k_4 s$$

with initial conditions

$$a(x,0) = a_0 \quad b(x,0) = 0 \quad m(x,0) = 0 \quad s(x,0) = 0,$$

and boundary conditions

$$a(0,t) = a_0 \quad a_x(L,t) = 0$$

$$b(L,t) = b_0 \quad b_x(0,t) = 0$$

$$m_x(0,t) = 0 \quad m_x(L,t) = 0$$

$$s_x(0,t) = 0 \quad s_x(L,t) = 0.$$

We scale the system by defining the following new variables:

$$\tilde{x} = \frac{x}{L} \quad \tilde{a} = \frac{a}{a_0} \quad \tilde{b} = \frac{b}{a_0} \quad \tilde{m} = \frac{m}{a_0} \quad \tilde{s} = \frac{s}{a_0} \quad \tau = \frac{t}{t_0}$$

where t_0 must be chosen. Here we consider two choices for t_0:

$$t_0 = \frac{1}{k_1 a_0} \tag{9}$$

$$t_0 = \frac{L^2}{D_a}. \tag{10}$$

Notice that both choices give us units of time since

$$[k_1] = \frac{cm^3}{mol * s}, \quad [a_0] = \frac{cm^3}{mol}, \quad [L] = cm, \text{ and } [D_a] = \frac{cm^2}{s}.$$

Thus τ will be unitless, as needed.

With Scaling (9), our system becomes

$$\frac{\partial \tilde{a}}{\partial \tau} = \frac{D_a}{L^2 k_1 a_0} \frac{\partial^2 \tilde{a}}{\partial \tilde{x}^2} - \tilde{a}\tilde{b}$$

$$\frac{\partial \tilde{b}}{\partial \tau} = \frac{D_b}{L^2 k_1 a_0} \frac{\partial^2 \tilde{b}}{\partial \tilde{x}^2} - \tilde{a}\tilde{b}$$

$$\frac{\partial \tilde{m}}{\partial \tau} = \frac{D_m}{L^2 k_1 a_0} \frac{\partial^2 \tilde{m}}{\partial \tilde{x}^2} + \tilde{a}\tilde{b} - \frac{k_2 a_0^{\nu-2}}{k_1} H(\tilde{m} - \eta)\tilde{m}^\nu - \frac{k_3}{k_1}\tilde{m}\tilde{s}$$

$$\frac{\partial \tilde{s}}{\partial \tau} = \frac{k_2 a_0^{\nu-2}}{k_1} H(\tilde{m} - \eta)\tilde{m}^\nu + \frac{k_3}{k_1}\tilde{m}\tilde{s} - \frac{k_4}{k_1 a_0}\tilde{s},$$

with initial conditions

$$\tilde{a}(\tilde{x}, 0) = 1 \quad \tilde{b}(\tilde{x}, 0) = 0 \quad \tilde{m}(\tilde{x}, 0) = 0 \quad \tilde{s}(\tilde{x}, 0) = 0,$$

and boundary conditions

$$\tilde{a}(0, \tau) = 1 \quad \tilde{a}_{\tilde{x}}(1, \tau) = 0$$

$$\tilde{b}(1, \tau) = \frac{b_0}{a_0} \quad \tilde{b}_{\tilde{x}}(0, \tau) = 0$$

$$\tilde{m}_{\tilde{x}}(0, \tau) = 0 \quad \tilde{m}_{\tilde{x}}(1, \tau) = 0$$

$$\tilde{s}_{\tilde{x}}(0, \tau) = 0 \quad \tilde{s}_{\tilde{x}}(1, \tau) = 0.$$

With Scaling (10), our system becomes

$$\frac{\partial \tilde{a}}{\partial \tau} = \frac{\partial^2 \tilde{a}}{\partial \tilde{x}^2} - \frac{k_1 a_0 L^2}{D_a}\tilde{a}\tilde{b}$$

$$\frac{\partial \tilde{b}}{\partial \tau} = \frac{D_b}{D_a}\frac{\partial^2 \tilde{b}}{\partial \tilde{x}^2} - \frac{k_1 a_0 L^2}{D_a}\tilde{a}\tilde{b}$$

$$\frac{\partial \tilde{m}}{\partial \tau} = \frac{D_m}{D_a}\frac{\partial^2 \tilde{m}}{\partial \tilde{x}^2} + \frac{k_1 a_0 L^2}{D_a}\tilde{a}\tilde{b} - \frac{k_2 a_0^{\nu-1} L^2}{D_a}H(\tilde{m} - \eta)\tilde{m}^\nu - \frac{k_3 a_0 L^2}{D_a}\tilde{m}\tilde{s}$$

$$\frac{\partial \tilde{s}}{\partial \tau} = \frac{k_2 a_0^{\nu-1} L^2}{D_a}H(\tilde{m} - \eta)\tilde{m}^\nu + \frac{k_3 a_0 L^2}{D_a}\tilde{m}\tilde{s} - \frac{k_4 L^2}{D_a}\tilde{s},$$

with initial conditions

$$\tilde{a}(\tilde{x},0) = 1 \quad \tilde{b}(\tilde{x},0) = 0 \quad \tilde{m}(\tilde{x},0) = 0 \quad \tilde{s}(\tilde{x},0) = 0,$$

and boundary conditions

$$\tilde{a}(0,\tau) = 1 \quad \tilde{a}_{\tilde{x}}(1,\tau) = 0$$

$$\tilde{b}(1,\tau) = \frac{b_0}{a_0} \quad \tilde{b}_{\tilde{x}}(0,\tau) = 0$$

$$\tilde{m}_{\tilde{x}}(0,\tau) = 0 \quad \tilde{m}_{\tilde{x}}(1,\tau) = 0$$

$$\tilde{s}_{\tilde{x}}(0,\tau) = 0 \quad \tilde{s}_{\tilde{x}}(1,\tau) = 0.$$

Both of these scalings are used throughout the literature. Authors such as Gálfi and Koza use Scaling (9) [10, 16], while others including Dee and Lebedeva use Scaling (10) [6, 17]. Generally, authors who are interested in studying the mathematical equations by themselves will use Scaling (9) since k_1 is a very large number, and this scaling will allow us to work with $\frac{1}{k_1}$, a small number, which is often easier to work with numerically. On the other hand, authors who are interested in comparing the model to experimental data will usually use Scaling (10). Since k_1 is generally just assumed to be very large, incorporating k_1 into our time scaling means that we do not have an accurate grasp on the units of time, and if we hope to compare our model to experimental data points, we will not be able to line up the time scaling correctly. Notice that in Scaling (10), D_a and L are the two quantities involved in the scaling, and for our experiment, these values are known. Therefore, we will be able to accurately match up our model's time scale with the time scale of experimental data. Since we hope to compare our model to experimental data, we will use Scaling (10) for the remainder of this thesis.

Now that we have a system of equations to model what we believe is occuring in our chemical reaction, we must of course test it. Ideally, we would like to be able to have data from our model match actual experimental data. Therefore in the next chapter, we will compare our model, both qualitatively and quantitatively to actual experimental data. If our model agrees with experimental data, we may then be able to use it to make predictions about future experiments and also possibly

to prove or disprove current theories on the NH$_3$-HCl reaction and on Liesegang ring formation in general.

4 Results

4.1 Prediction of the First Band Position

Recall from Section 2.4 that this experiment is used as a high school demonstration of Graham's Law of Diffusion. Recall that if we can show, in the counter-diffusional case, that the first band can be formed at several places along the tube simply by varying our boundary conditions, then we will have supported the idea that this experiment should not be used as a high school demonstration of Graham's Law of Diffusion. So let us then discuss the position of the first band.

Using experimental data from two separate experiments [32] in combination with our model, we can calculate η, the homogeneous nucleation threshold value, and we can also calculate the heterogeneous nucleation threshold value. We do so by running the model up to the time of heterogeneous and homogeneous nucleation (given by Thompson's experimental data [32]) and observing the monomer concentration value at each of these time points. In Table 1, we see these values calculated from the model using the experimental data from the first experiment. We then also record the position along the tube where these thresholds occur so that we may talk about the position of the first band formation. All simulations of the model are carried out by the MATLAB pdepe solver, which uses a spatial discretization described by Skeel and Berzins [29] and the MATLAB ode15s solver developed by Shampine et. al [25, 26] for time integration.

We can see where homogeneous and heterogeneous nucleation occurs in Figure 18, which depicts front position as a function of time. It is important to note that we have chosen to model the front position as the position along the tube of the maximum amount of monomer present. We obtain similar information from the second experiment as shown in Table 2 and Figure 19.

From Tables 1 and 2, we observe that the homogeneous nucleation threshold values, which average to 0.0394 mm Hg and 0.0441 mm Hg, are consistent with those of Twomey [33]. From

Table 1: Thresholds Experiment 1 [32]

	Experimental Data			Model		
$\dfrac{\mathrm{PP}_{NH_3}}{\mathrm{PP}_{HCl}}$	Time to Het. Nuc. (min.)	Time to Hom. Nuc. (min.)	Position of Hom. Nuc. (divided by L)	Het. Nuc. Threshold (mm Hg)	Hom. Nuc. Threshold (mm Hg)	Position of Hom. Nuc. (divided by L)
4.3445	8.20	9.68	0.41625	0.0038	0.02296	0.4070
0.6280	8.54	11.05	0.46667	0.0017	0.0237	0.4600
0.3470	8.98	11.49	0.47	0.0020	0.0228	0.4700
0.1683	9.895	12.64	0.48542	0.0037	0.0303	0.4860
0.0805	9.97	13.33	0.5154	0.0024	0.0278	0.5000
0.0360	13.03	15.57	0.53542	0.0141	0.0446	0.5260
0.0174	12.78	16.22	0.5725	0.0074	0.0349	0.5440
0.0080	15.85	20.53	0.62167	0.0180	0.0652	0.5880
0.0035	19.25	23.95	0.67917	0.0278	0.0672	0.6320
0.0017	20.215	26.32	0.7075	0.0206	0.0544	0.6720
			Average Values	0.0102	0.0394	
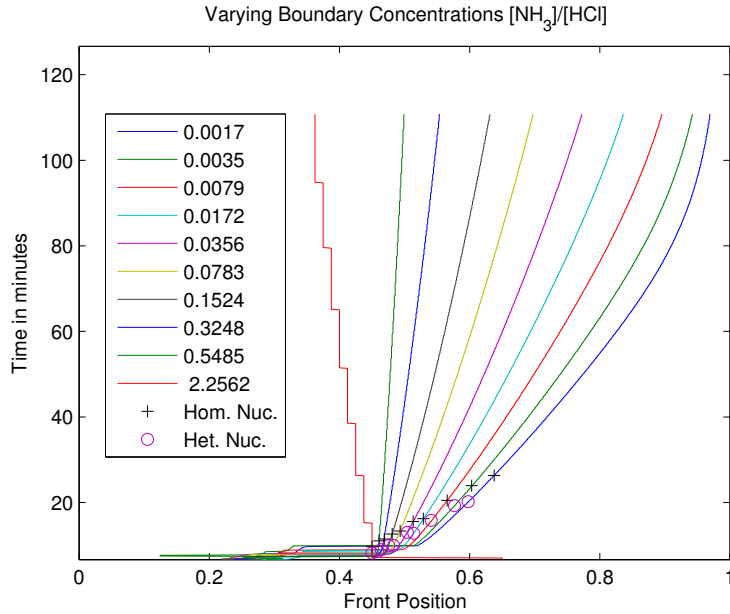
Figure 18: Experiment 1: Front position, homogeneous and heterogeneous nucleation thresholds at varying boundary concentrations. Note that the data with concentration ratio 2.2562 could only be obtained using a smaller number of space steps.

27

Table 2: Thresholds Experiment 2 [32]

Experimental Data				Model		
$\dfrac{\mathrm{PP}_{NH_3}}{\mathrm{PP}_{HCl}}$	Time to Het. Nuc. (min.)	Time to Hom. Nuc. (min.)	Position of Hom. Nuc. (divided by L)	Het. Nuc. Threshold (mm Hg)	Hom. Nuc. Threshold (mm Hg)	Position of Hom. Nuc. (divided by L)
50.5319	9.785	11.75	0.35417	0.0071	0.028	0.375
10.5102	10.22	14.30	0.37792	0.0038	0.061	0.39
5.8061	11.515	15.28	0.40417	0.0072	0.045	0.41
2.8163	11.90	16.91	0.4262	0.0062	0.051	0.473
1.3469	13.44	17.17	0.45875	0.0095	0.0392	0.4440
0.4191	16.87	18.30	0.49917	0.0187	0.02842	0.4740
0.2021	15.73	23.72	0.52583	0.0083	0.05586	0.5020
			Average Values	0.0087	0.0441	
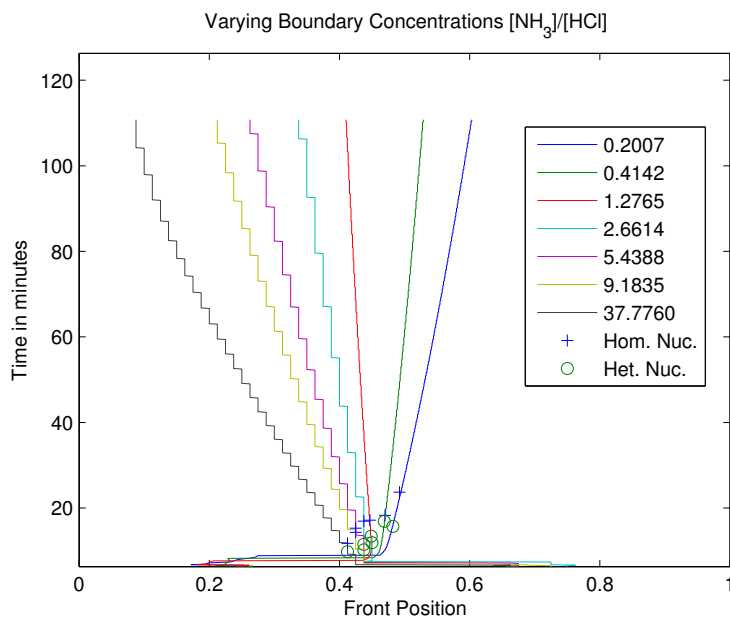
Figure 19: Experiment 2: Front position, homogeneous and heterogeneous nucleation thresholds at varying boundary concentrations. Note that the data with concentration ratios 2.6614, 5.4388, 9.1835, and 37.7760 could only be obtained using a smaller number of space steps.

Figures 18 and 19, we first notice that the front will move in different directions depending on the boundary concentrations. This is consistent with experimental data [32].

As stated above, though, we are interested in finding the position of the first band that is formed. As discussed in Section 2.2, the first band is formed when the monomer concentration increases about a certain threshold, which we call η. Since we have calculated this value in Tables 1 and 2 and plotted it in Figures 18 and 19, we can see that the homogeneous nucleation occurs, not at one spot, but at various positions along the tube. Experimental data agrees with this conjecture, as shown in the 'Position of Homogeneous Nucleation' column in Tables 1 and 2, where positions have been scaled by L and measured as the distance from the HCl side of the tube. Therefore, we can say with certainty that the traditional NH_3-HCl high school demonstration of Graham's Law of Diffusion has its flaws.

4.2 Prediction of the Final Band Position

Let us now consider the problem of finding the position of the last ring, i.e., where the reaction front will reach equilibrium and stop moving. Consider the equations that affect the position of the front

$$a_t = D_a \frac{\partial^2 a}{\partial x^2} - k_1 ab$$
$$b_t = D_b \frac{\partial^2 b}{\partial x^2} - k_1 ab$$
$$m_t = k_1 ab.$$

So let $t \to \infty$ so that $a_t = 0$, $b_t = 0$, and $m_t = 0$, as is the case in chemical equilibrium. Then we have

$$0 = D_a \frac{\partial^2 a}{\partial x^2} - k_1 ab$$
$$0 = D_b \frac{\partial^2 b}{\partial x^2} - k_1 ab$$
$$0 = k_1 ab,$$

or equivalently

$$0 = D_a \frac{\partial^2 a}{\partial x^2} = \frac{\partial}{\partial x}\left(D_a \frac{\partial a}{\partial x}\right)$$

$$0 = D_b \frac{\partial^2 b}{\partial x^2} = \frac{\partial}{\partial x}\left(D_b \frac{\partial b}{\partial x}\right).$$

Notice that $\frac{\partial^2 a}{\partial x^2} = 0$ and $\frac{\partial^2 b}{\partial x^2} = 0$ since D_a, $D_b > 0$. Therefore at the position of the final ring (when the system is in equilibrium), the concentration profiles of our reactants must be linear, as in Figure 20.
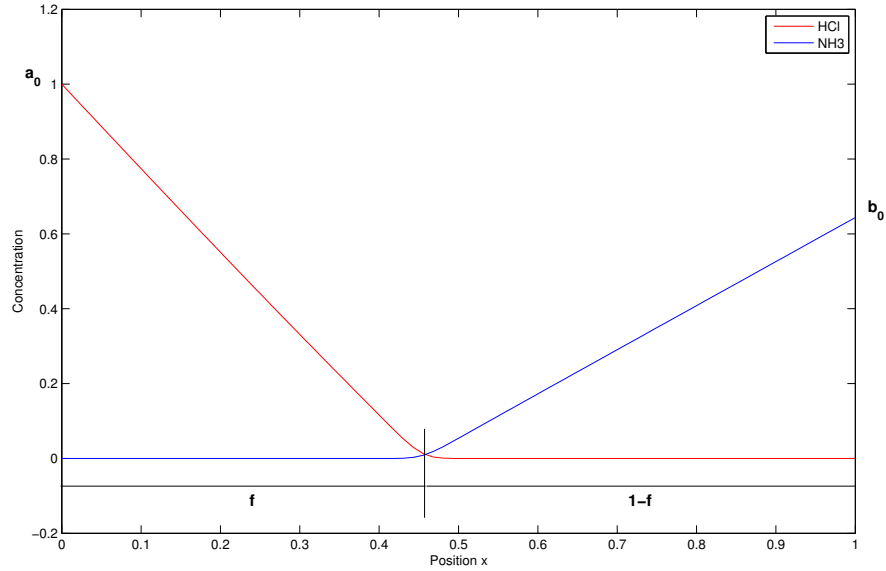
Figure 20: Concentration profiles of HCl and NH$_3$ when the reaction front has reached its final position. Here, the system is at equilibrium.

If we remember that $a = [HCl]$ and $b = [NH_3]$, then we can see from Figure 20 that we obtain the following equations:

$$a = a_0 - \frac{a_0}{f}x \tag{11}$$

$$b = b_0 + \frac{b_0}{1 - f}x. \tag{12}$$

At the reaction front, we know that the fluxes of the two diffusing chemicals must be equal, and

30

so we have

$$- \text{ Flux of } a = -D_a\frac{\partial a}{\partial x} = D_b\frac{\partial b}{\partial x} = \text{ Flux of } b.$$

Since $\frac{\partial a}{\partial x} = -\frac{a_0}{f}$ and $\frac{\partial b}{\partial x} = \frac{b_0}{1-f}$ by (11) and (12), now we have

$$D_a\frac{a_0}{f} = D_b\frac{b_0}{1-f}.$$

Solving for f, we obtain

$$f = \frac{D_a a_0}{D_a a_0 + D_b b_0} = \frac{\frac{D_a}{D_b}}{\frac{D_a}{D_b} + \frac{b_0}{a_0}} = \frac{1}{1 + \frac{D_b b_0}{D_a a_0}}.$$

Therefore, as long as we know the diffusion coefficients and the concentrations of our chemicals, we can predict the position of the final ring, the place where the reaction front will stop moving.

Let us, for a moment, consider what is happening before this final ring. We know that up until this final ring is formed, the reaction front is moving and, depending on the conditions, precipitate rings may be formed and deposited along the way. We would like to be able to access all of the possible conditions under which this occurs.

Notice that in the case where the tube is initially flooded with HCl and then the NH_3 diffuses into the tube, we will start with very large fluxes into the reaction zone, and eventually the flux of both chemicals will decrease until it reaches its final equilibrium state. Recalling that the slopes of the concentration profiles ($\frac{\partial \phi}{\partial x}$) at the reaction zone are proportional to the fluxes ($D_\phi\frac{\partial \phi}{\partial x}$), Figure 21 exhibits the transition from a large initial flux decreasing to its final equilibrium state.

Now if we turn our attention to the counter-diffusion experiment where we don't flood the tube with HCl but rather we let the two gases diffuse into the tube, here we see that we begin with a very small flux into the reaction zone, and the flux gradually increases until we reach the final state. Again, if we remember that the slopes of the concentration profiles ($\frac{\partial \phi}{\partial x}$) are proportional to the fluxes of the respective chemicals, we can see in Figure 22 that the slope/flux will start off small and then gradually increase until we reach the final equilibrium state.

We had hoped that we would be able to demonstrate all possible outcomes of our experiment. Notice that, through the flooded tube case and the counter-diffusion case, we can access all possible
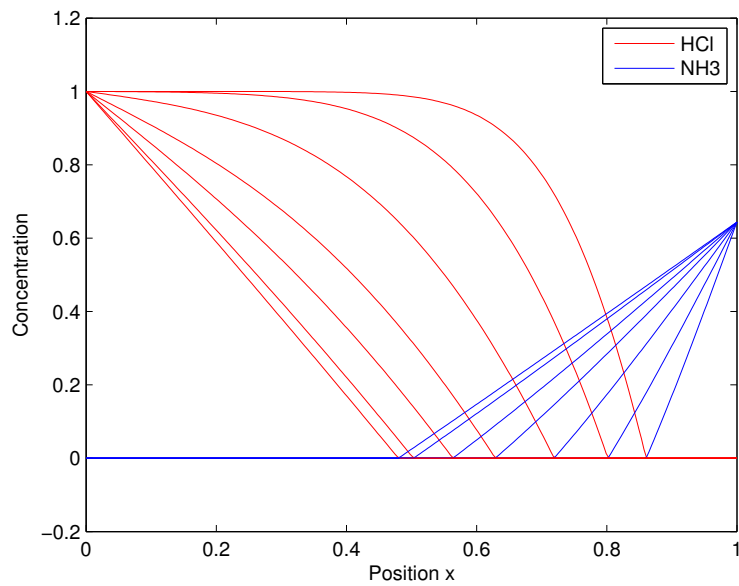
Figure 21: Concentration profiles of HCl and NH$_3$ at various times in the flooded tube experiment. Notice that, initially, both concentration profiles have a very steep slope at the reaction front. Then the front moves until it reaches its final position when the concentration profiles are linear.
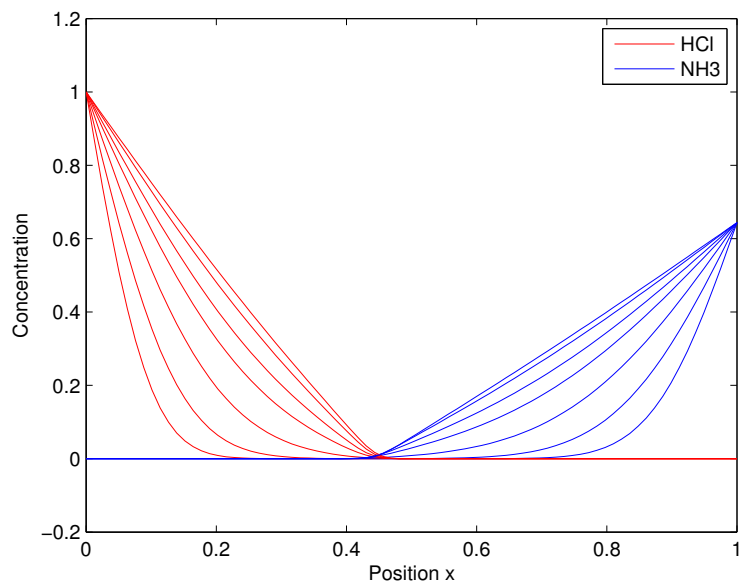
Figure 22: Concentration profiles of HCl and NH$_3$ at various times in the counter-diffusional experiment. Notice that, initially, both concentration profiles have a very shallow slope at the reaction front. Then the front moves until it reaches its final position when the concentration profiles are linear.

fluxes into the reaction zone. In the flooded tube case, we go from a high flux into the reaction zone to the final equilibrium state while in the couter-diffusion case, we begin with a small flux and increase to the final equilibrium state. So, in conclusion, we now have predictions for positions of the first and final band formation, as well as access to all possible fluxes into the reaction zone.

4.3   Effect of the tube length L

Now we turn our attention to the effect of the tube length L in our model. Let us first consider the effect of L on the front position. We will focus on the first two equations in our model:

$$a_t = D_a a_{xx} - kab$$

$$b_t = D_b b_{xx} - kab,$$

with boundary conditions

$$a(0, t) = a_0 \qquad a_x(L, t) = 0$$

$$b_x(0, t) = 0 \qquad b(L, t) = b_0$$

and initial conditions

$$a(x, 0) = 0 \qquad b(x, 0) = 0.$$

If we rescale our model using

$$\tilde{a} = \frac{a}{a_0} \qquad \tilde{b} = \frac{b}{a_0}$$

while defining the following

$$D = D_a = D_b \qquad c = \tilde{b} - \tilde{a},$$

then we obtain a new model in just one variable:

$$c_t = Dc_{xx}$$

$$c(0,t) = -1 \quad c(L,t) = \frac{b_0}{a_0} = r_0$$

$$c(x,0) = 0.$$

We see that we have the diffusion equation with inhomogeneous, constant, Dirichlet boundary conditions. Therefore we can find a solution $c(x,t)(= \tilde{b}(x,t) - \tilde{a}(x,t)) =$

$$r_0 \left[\frac{x}{L} + \sum_{n=1}^{\infty} \frac{2(-1)^n}{n\pi} \exp\left(\frac{-n^2\pi^2 Dt}{L^2} \right) \sin\left(\frac{n\pi x}{L} \right) \right] + \left[\frac{x}{L} - 1 + \sum_{n=1}^{\infty} \frac{2}{n\pi} \exp\left(\frac{-n^2\pi^2 Dt}{L^2} \right) \sin\left(\frac{n\pi x}{L} \right) \right].$$

Then we can scale this equation by the following:

$$\tilde{x} = \frac{x}{L} \qquad \tau = \frac{t}{\frac{L^2}{D}}.$$

Using this scaling, we obtain the solution $c(\tilde{x}, \tau) = \tilde{b}(\tilde{x}, \tau) - \tilde{a}(\tilde{x}, \tau) =$

$$r_0 \left[\tilde{x} + \sum_{n=1}^{\infty} \frac{2(-1)^n}{n\pi} \exp\left(-n^2\pi^2 \tau \right) \sin\left(n\pi\tilde{x} \right) \right] + \left[\tilde{x} - 1 + \sum_{n=1}^{\infty} \frac{2}{n\pi} \exp\left(-n^2\pi^2 \tau \right) \sin\left(n\pi\tilde{x} \right) \right]. \quad (13)$$

Notice in Figures 23 and 24 that we can now obtain solutions for $a(x,t)$ and $b(x,t)$, as well as the front position as a function of time $s(t)$. In order to do so, we must assume that the front position occurs exactly when $c(x,t) = 0$. Then, since our two gases a and b diffuse from opposite ends of the tube, then $b(x,t) = 0$ to the left of the front position, where $c(x,t) = 0$ and $a(x,t) = 0$ to the right of the front position. Therefore the solution $b(x,t) = c(x,t)$ to the right of the front position, and $a(x,t) = c(x,t)$ to the left of the front position.

Also, from our solution (13), notice that we have scaled out the tube length L. So for the case when our diffusion coefficients are equal $(D_a = D_b)$, we can predict exactly the effect of the tube length on our experiment. Specifically, we can predict the effect that tube length has on the front position.

Now, for the case when the diffusion coefficients are not equal $(D_a \neq D_b)$, we refer back to Section 3.6 to the nondimensionalized model using Scaling (10). Notice that the tube length L has
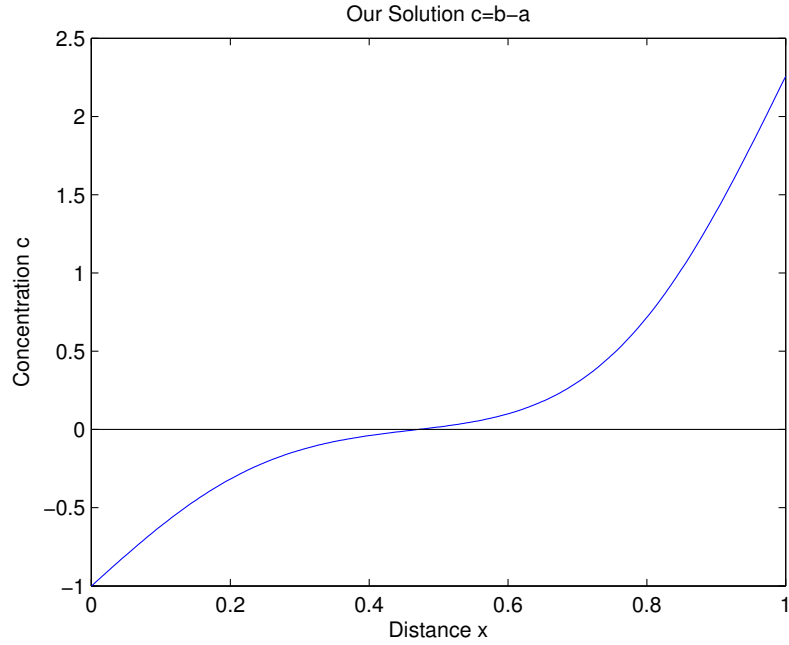
Figure 23: Plot of the solution $c(\tilde{x}, \tau) = \tilde{b}(\tilde{x}, \tau) - \tilde{a}(\tilde{x}, \tau)$. Here, $a_0 = 164$, $b_0 = 370$, $D = 0.13$, and $\tau = 0.02$ (about 37 min.). Notice that to the left of the point where $c = 0$, we have a solution for $-\tilde{a}$, and to the right of the point where $c = 0$, we have a solution for $\tilde{b}$.
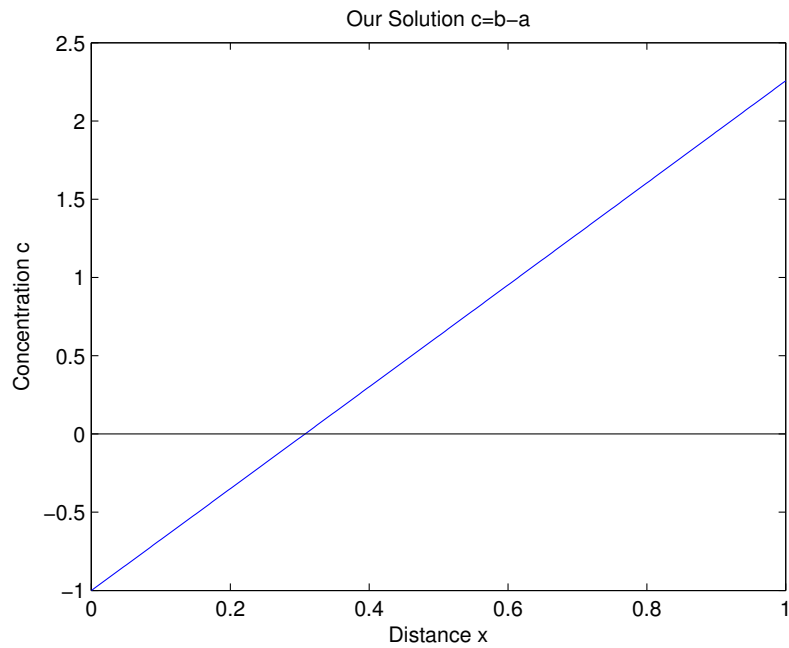
Figure 24: The final equilibrium state of the solution $c(\tilde{x}, \tau) = \tilde{b}(\tilde{x}, \tau) - \tilde{a}(\tilde{x}, \tau)$. Here, $a_0 = 164$, $b_0 = 370$, $D = 0.13$, and $\tau = 0.6$. Notice that our final state is linear, as discussed in Section 4.2.

35

again been absorbed in our scaling; however, if we examine the first two equations in our model after the rescaling, we see that L still remains. In other words, L was not completely absorbed as it was in (13) where $D_a = D_b$. Notice though that L can, in a sense, be absorbed by k_1 since we know that k_1 is large. Therefore multiplying k_1 by L^2 will have a very little effect, macroscopicallly. Now if we were to study this system at the microscopic level, we would have to consider the effect of multiplying k_1 by L^2. Since we are currently concerned with front position, we can again predict the effect that the tube length L has on the front position.

Another important thing to note about our solution (13) is that even when $D_a = D_b$, we can change our solution by inputting different values for a_0 and b_0. By changing a_0 and/or b_0, we will change $r_0 = \frac{b_0}{a_0}$, which therefore changes our solution. Therefore, we can say with certainty that a_0 and b_0 have an effect on this experiment, and so we can alter the outcome of the experiment, simply by changing the concentrations at the end of our tube.

4.4 Front Velocity in the Flooded Tube Experiment

Using data from Lenczycki's flooded tube experiment [18], we can also compare front velocities of our model to actual experimental data. Notice in Table 3, that we get a nice correlation between actual experimental data and what the model predicts.

Table 3: Front Velocity [18]

Time Segment (s)	Experimental Data (cm/s)	Model (cm/s)
195-215	0.014210	0.0154
300-325	0.0094554	0.0093
380-420	0.0065864	0.0077
470-495	0.0048210	0.00456
635-665	0.0025081	0.0026
1000-1030	0.0011244	0

4.5 Width of Heterogeneous Nucleation Zone

We noted back in Section 2.4, specifically in Figure 9, that we can measure the width of the heterogeneous nucleation zone. Let us then consider some predictions from our model about the width of this zone.
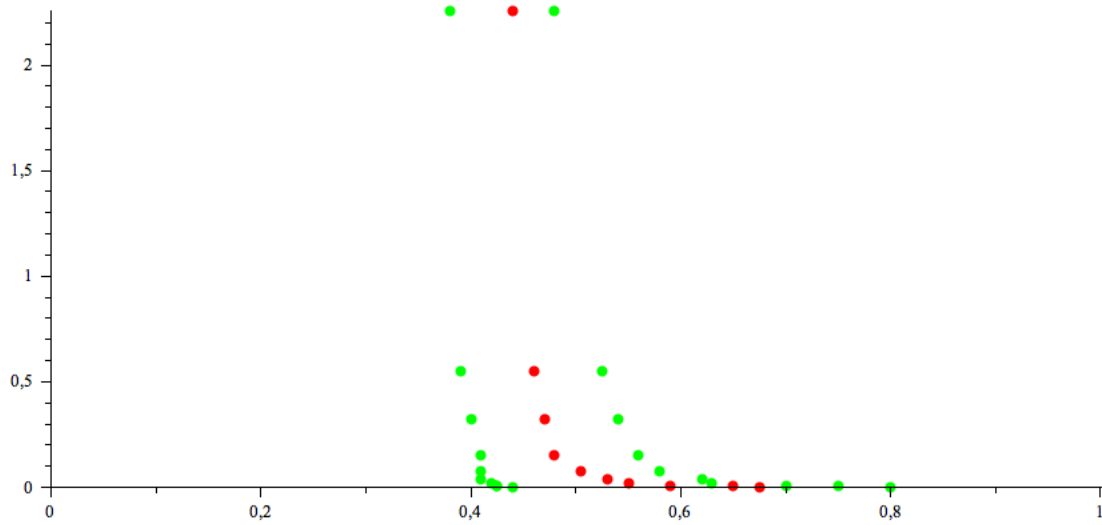
Figure 25: Position in tube (horizontal axis) vs. Concentration ratio (vertical axis). The red dots represent the position of homogeneous nucleation at varying concentrations while the distance between the green dots represents the width of the heterogeneous nucleation zone, as calculated by the model.
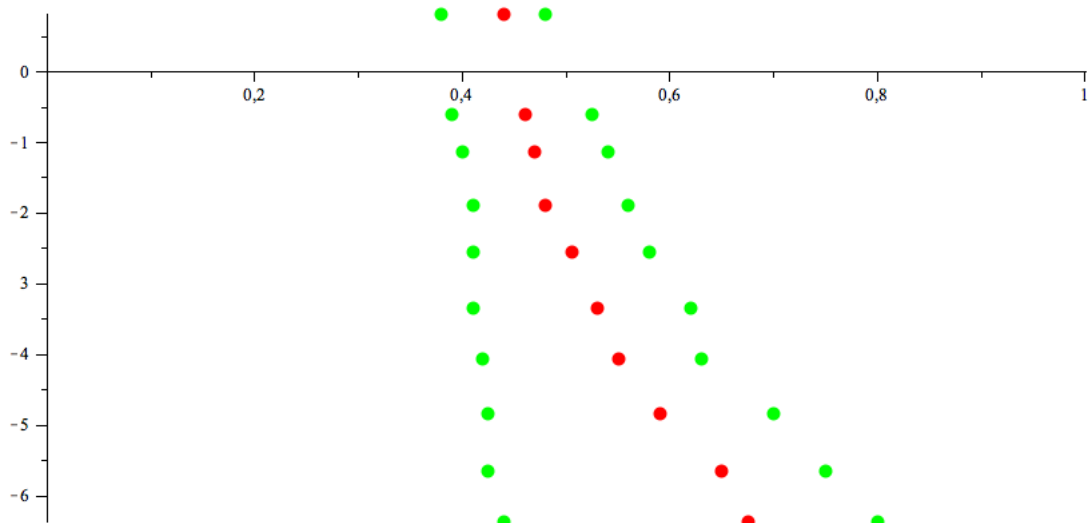
Figure 26: Position in tube (horizontal axis) vs. Log of the concentration ratio (vertical axis). The red dots represent the position of homogeneous nucleation at varying concentrations while the distance between the green dots represents the width of the heterogeneous nucleation zone, as calculated by the model.

Notice that in Figure 25, we have plotted the width of the heterogeneous nucleation zone at varying concentration ratios, as indicated by the distance between the green dots. Since we have threshold values for heterogeneous and homogeneous nucleation, we examined the monomer concentration profile from the time it increases above the heterogeneous nucleation threshold to the time it hits the homogeneous nucleation threshold. The width of the zone is then measured by the width of the monomer concentration profile that is above this heterogeneous nucleation threshold exactly at the time when the peak of the monomer concentration hits the homogeneous nucleation threshold. In Figure 26, we just consider the Log of the concentration ratio so that we may see the individual widths more clearly.

Notice that as our concentration ratio $(\frac{PP_{NH_3}}{PP_{HCl}})$ decreases, the width of our heterogeneous nucleation zone increases. This is consistent with what we have observed experimentally.

4.6 Effect of Water Vapor on the System

In Section 3.4, we made the assumption that $k_1 >> D_a, D_b$ [9, 30], based on what was found in the literature; however, we found somewhat contradictory information from Countess and Heicklen. They stated that $k_1 = 1.9 \cdot 10^{-17} \frac{cm^3}{sec \cdot molecule}$ for the NH$_3$ - HCl reaction [5]. Even when we convert this number to the units that we use in our model, we still get a small number:

$$ k_1 = 1.9 \cdot 10^{-17} \ \frac{\text{cm}^3}{\text{sec} \cdot \text{molecule}} = 0.6 \ \frac{1}{\text{sec} \cdot \text{mmHg}}. $$

It is important to note that this k_1, given by Countess and Heicklen, was calculated for *anhydrous* conditions. If we were to use this k_1 in our model, we would not get the values that agree with experimental data, as we did in Section 4.1. It is only when we increase k_1 up to much higher values that we get the desired result. Therefore, we can say with certainty that water vapor is an extremely important catalyst in this reaction and must be considered as part of the mechanism behind this system.

5 Conclusion and Future Work

In summary, we have examined the theory behind Liesegang rings, specifically the NH_3-HCl system, and we have derived and presented a pre-nucleation model for the NH_3-HCl system. Data obtained from this model has been compared with experimental data, and this data has been used to predict the position of the first band of solid precipitate. We have also predicted the position of the final precipitation band and examined the effect of the tube length L. In the case of a flooded tube, we have compared front velocity experimental data with data obtained from the model. We have examined the width of the heterogeneous nucleation zone, and finally, we have discussed the effect of water vapor on the system.

While we have found answers to many of the questions that we wanted to answer, there are still many more issues that we would like to address. First, we are able to obtain nice information about the formation of the monomer. From Figure 27, we can see the increase and decrease in monomer concentration at the front. We would like to be able to match the amplitude and frequency of these oscillations to those obtained by Lenczycki [18].

We would also like to improve the numerical techniques used. From Section 4.3, we would like to use our solutions $a(x,t)$ and $b(x,t)$ and plug them into the m_t and s_t equations in our model. Then, instead of trying to solve four partial differential equations numerically at one time, we could simply work with the last two equations. Recall, from Section 4.3, that our solutions for $a(x,t)$ and $b(x,t)$ assume that the front position occurs exactly at one point. Since we know that this is not the case, we will model the width of the front position and incorporate that into our solutions $a(x,t)$ and $b(x,t)$.

Now that we have threshold values for heterogeneous nucleation, we would like to incorporate a heterogeneous nucleation threshold in our model as well. Also, it has been observed that the width of the heterogeneous nucleation zone, as shown in Figure 9, varies as the boundary conditions
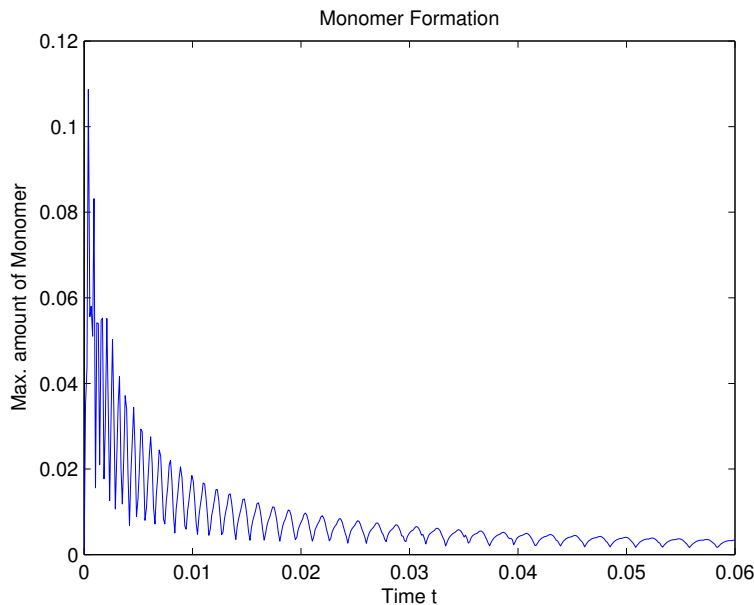
Figure 27: Monomer concentration at the reaction front. We can think of the oscillations as band formation caused by the nucleation threshold in the J-curve.

vary, as discussed in Section 4.5. We would like to obtain experimental data on the width of the heterogeneous nucleation zone so that we may compare it to the data obtained by the model.

We would also like to note that our model is a pre-nucleation model, based on pre-nucleation events. Several sources state that pre-nucleation models, by themselves, are insufficient in describing Liesegang rings [9, 11, 13, 19, 22, 24]. Post-nucleation events include things such as phase separation and something called Ostwald Ripening where large solid particles aggregate more quickly than smaller particles. These events occur after nucleation and can certainly be incorporated into our model. In fact, some have used the Cahn-Hilliard equation to model the phase separation that occurs [11, 23].

We discuss the effect of tube length in Section 4.3, but in our model, it is important to note that we ignore the effect of tube diameter. This is because our model is only a one-dimensional model; however, it has been observed that different diameters affect the experiment. Mason and Kronstadt suggest that this is due to convection [20]. Certainly, this is something which should be investigated and included in the model.

Looking back at Figure 13 and the figures that lead up to it, we see a depletion zone in the heterogeneous nucleation begin to widen, and we see the first step in band formation, a small patch

40

of light. We may ask ourselves what causes this depletion zone to occur and then widen? We believe that thermophoresis and/or diffuseophoresis may be the cause, that heat given off from the reaction may cause the heterogeneously nucleated particles to move away from the reaction front. We would like to explore this idea further.

We are also interested in modeling the effect of the water vapor on the system. As discussed in Section 4.6, water vapor certainly will have an effect on the system, and we currently do not have anything in model describing this effect. We are also interested in modeling the effect of ions and radicals in the system since it has been observed that ions and radicals actually reduce the nucleation threshold of the NH_3-HCl reaction [3].

If we essentially turn our NH_3-HCl tube on its side so that it is now positioned as an upright cylinder and if we place a drop of ammonia at the bottom and a drop of hydrochloric acid at the top, the ammonia will diffuse up towards the hydrochloric acid drop until a reaction front is formed as shown in Figure 28. In this set-up, the reaction front forms around the drop of hydrochloric acid, and if we look at a top-view of this system as in Figure 29, we see that Liesegang rings form as the reaction front moves away from the drop of HCl.

We also have experimental data for the position of the front, where small oscillations occur [18]. Fourier analysis of this data shows period doubling and eventually chaotic behavior of these oscillations [28]. We are interested in studying this further.

Finally, we would like to turn our studies to a starch-iodine system, which seems to exhibit behavior similar to that of the NH_3-HCl system. The equations from our model could potentially be used to describe certain behaviors of the starch-iodine system as well.

Figure 28: The ammonia diffuses up and forms a reaction front near the HCl drop.

Figure 29: A top view of the HCl drop. Liesegang rings are formed as the reaction front moves.

REFERENCES

[1] T. Antal, M. Droz, J. Magnin, Z. Racz, and M. Zrinyi. Derivation of the matalon-packter law for liesegang patterns. *J. Chem. Phys.*, 109:9479, 1998.

[2] U. Baltensperger. Aerosols in clearer focus. *Science*, 329(5998):1474–1475, 2010.

[3] C. M. Banic and J. V. Iribarne. Nucleation of ammonium chloride in the gas phase and the influence of ions. *J. Geophys. Res.*, 85(C12):7459–7464, 1980.

[4] B. Chopard, M. Droz, T. Karapiperis, and Z. Rácz. Properties of the reaction front in a reversible $A + B \rightleftharpoons C$ reaction-diffusion process. *Phys. Rev. E*, 47:R40–R43, Jan 1993.

[5] R. J. Countess and J. Heicklen. Kinetics of particle growth. II. Kinetics of the reaction of ammonia with hydrogen chloride and the growth of pariculate ammonium chloride. *The Journal of Physical Chemistry*, 77(4):444–447, 1973.

[6] G. T. Dee. Patterns produced by precipitation at a moving reaction front. *Phys. Rev. Lett.*, 57:275–278, Jul 1986.

[7] N.A. Dimmock and G.B. Marshall. The determination of hydrogen chloride in ambient air with diffusion/denuder tubes. *Analytica Chimica Acta*, 202(0):49 – 59, 1987.

[8] M. Droz, J. Magnin, and M. Zrinyi. Liesegang patterns: Studies on the width law. *The Journal of Chemical Physics*, 110(19):9618–9622, 1999.

[9] M. A. Einarsrud, F. A. Maaø, A. Hansen, M. Kirkedelen, and J. Samseth. Band formation during gaseous diffusion in aerogels. *Phys. Rev. E*, 57:6767–6773, Jun 1998.

[10] L. Gálfi and Z. Rácz. Properties of the reaction front in an $A + B \rightarrow C$ type reaction-diffusion process. *Phys. Rev. A*, 38:3151–3154, Sep 1988.

[11] P. Hantz. *Pattern Formation in a New Class of Precipitation Reactions*. PhD thesis, University of Geneva, 2006.

[12] H. H. Hickam, Jr. *Rocket Boys*. Delacorte Press, 1998.

[13] H. Higuchi and R. Matuura. The concentration distribution of ions in the gel before the periodic precipitation. *Faculty of Science, Kyushu University, Series C*, 5(2):33–42, 1962.

[14] C.K. Jablczynski. La formation rythmique des prècipitès: Les anneaux de liesegang. *Bulletin del la Societè Chimique de France*, 33:1592–1603, 1923.

[15] Z. Koza. Numerical analysis of reversible $A + B \leftrightarrow C$ reaction-diffusion systems. *European Physical Journal B*, 32:507–511, April 2003.

[16] Z. Koza. Reaction fronts in reversible $A + B \rightleftharpoons C$ reaction-diffusion systems. *Physica A: Statistical Mechanics and its Applications*, 330(12):160 – 166, 2003.

[17] M. I. Lebedeva, D. G. Vlachos, and M. Tsapatsis. Bifurcation analysis of liesegang ring pattern formation. *Phys. Rev. Lett.*, 92:088301, Feb 2004.

[18] T. T. Lenczycki. Oscillations in gas phase periodic precipitation systems: The NH_3-HCl story. Master's thesis, Spring 2003.

[19] K. Martens. *Investigation of Non-Equilibrium Systems: Validity of Generalized Equilibrium Concepts and Control of Precipitation Patterns*. PhD thesis, University of Geneva, 2009.

[20] E. A. Mason and B. Kronstadt. Graham's laws of diffusion and effusion. *Journal of Chemical Education*, 44(12):740, 1967.

[21] H. W. Morse and G. W. Pierce. Diffusion and supersaturation in gelatine. *Phys. Rev. (Series I)*, 17:129–150, Sep 1903.

[22] S. C. Müller and J. Ross. Spatial structure formation in precipitation reactions. *The Journal of Physical Chemistry A*, 107(39):7997–8008, 2003.

[23] Z. Rácz. Formation of Liesegang patterns. *Physica A Statistical Mechanics and its Applications*, 274:50–59, December 1999.

[24] J. Ross. Formation of spatial structures in chemical reactions. *Physica D: Nonlinear Phenomena*, 12(13):303 – 304, 1984.

[25] L. F. Shampine and M. W. Reichelt. The MATLAB ODE Suite. *SIAM Journal on Scientific Computing*, 18(1):1–22, 1997.

[26] L. F. Shampine, M. W. Reichelt, and J. A. Kierzenka. Solving Index-1 DAEs in MATLAB and Simulink. *SIAM Review*, 41(3):538–552, 1999.

[27] A. H. Sharbaugh and A. H. Sharbaugh. An experimental study of the Liesegang phenomenon and crystal growth in silica gels. *Journal of Chemical Education*, 66(7):589, 1989.

[28] J. Shinn. Chemical kinetics and the Rössler system. *Dynamics at Horsetooth*, 2B, 2010.

[29] R. D. Skeel and M. Berzins. A method for the spatial discretization of parabolic equations in one space variable. *SIAM Journal on Scientific and Statistical Computing*, 11(1):1–32, 1990.

[30] D. Smith. On Ostwald's supersaturation theory of rhythmic precipitation (Liesegang's rings). *The Journal of Chemical Physics*, 81(7):3102–3115, 1984.

[31] L. L. Spiller. Determination of ammonia/air diffusion coefficient using nafion lined tube. *Analytical Letters*, 22(11-12):2561–2573, 1989.

[32] S. Thompson. Personal communication to be published, 1994.

[33] S. Twomey. Nucleation of ammonium chloride particles from hydrogen chloride and ammonia in air. *The Journal of Chemical Physics*, 31(6):1684–1685, 1959.